PHILOSOPHICAL MAGAZINE A, 2001, VOL. 81, NO. 2, 399–415

Cyclic deformation behaviour of a copper bicrystal with common primary slip planes

Z. F. ZHANG† and Z. G. WANG

State Key Laboratory for Fatigue and Fracture of Materials, Institute of Metal Research, Chinese Academy of Sciences, Shenyang, 110015, PR China

[*Received 27 January 2000 and accepted 3 May 2000*]

ABSTRACT

Cyclic deformation behaviour of a $[\bar{4}\,15\,20]$-$[18\,\bar{2}\,7]$ copper bicrystal with a tilting $\Sigma = 19b$ grain boundary (GB) was investigated in the axial plastic strain range 1.5×10^{-4}-2.13×10^{-3} at room temperature in air. The primary slip planes (111) within the $\mathbf{G}_1[\bar{4}\,15\,20]$ and $\mathbf{G}_2[\bar{1}8\,\bar{2}\,7]$ grains in the bicrystal were designed to be coplanar in order to reveal the interaction of slip bands with the GB. The results show that the cyclic stress-strain curve of the bicrystal displays a plateau region with axial saturation stresses of 61.6–63.5 MPa over the applied strain range. This result is similar to that for a single-slip-oriented copper single crystal, indicating that the GB has little effect on the saturation stress. After cyclic deformation, the surface morphology of the bicrystal exhibits the following features. Firstly, only the primary slip system was activated in both grains. Secondly, the primary slip bands on the four surfaces of the two grains show a good one-to-one relationship across the GB, indicating that surface slip bands can transfer through it. Thirdly, secondary slip systems were not activated, even in the vicinity of the GB. Dislocation patterns of the bicrystal were observed by the electron channelling contrast technique. The two-phase structure of persistent slip bands (PSBs) and matrix (or veins) formed in both grains. The ladder-like PSBs were observed to transfer through the GB continuously on one surface of the bicrystal but piled-up at the GB on the other surface, showing a discontinuous dislocation distribution next to the GB. Several kinds of interaction between dislocations and the GB were observed on the common slip plane. The cyclic stress–strain response and the interactions between dislocations, PSBs and the GB are discussed.

§1. INTRODUCTION

Copper single crystals were widely investigated as model materials to reveal the fatigue damage mechanism of materials (Mughrabi 1978, Basinski and Basinski 1992, Laird *et al*. 1986, Laird 1996). All these investigations reveal that almost all the plastic strain is carried by persistent slip bands (PSBs), which consist of thin lamellae extending in the bulk through the specimens. In particular, the PSBs are composed of nearly parallel and narrow dislocation walls arranged in fairly equal spacing perpendicular to the primary Burger vector and are embedded in a matrix structure of loop patches. This feature was well explained by Winter (1974) and Finney and Laird (1975) in terms of a two-phase model (PSB and matrix). Correspondingly, the fatigue damage mechanism of copper single crystals is always

† Author for correspondence. Email: zhfzhang@imr.ac.cn.

Philosophical Magazine A ISSN 0141–8610 print/ISSN 1460-6992 online
http://www.tandf.co.uk/journals

associated with the formation of PSBs at low or intermediate strain amplitudes (Essmann *et al*. 1981, Hunsche and Meumann 1986, Basinski and Basinski 1989, 1992, Repetto and Ortiz 1997).

It was also observed that the dislocation structures characteristic of PSB form in the interior of polycrystalline copper (Winter *et al*. 1981, Pedersen *et al*. 1982). However, the fatigue damage mechanisms of polycrystals are quite different from those of single crystals because grain boundaries (GBs) act as obstacles against slip deformation and often become the preferential site of fatigue crack initiation during cyclic deformation (Swearengen and Taggart 1971, Waltersdorf and Vehoff 1989). Therefore, in recent studies, copper bicrystals were employed to clarify the GB effect on fatigue damage by Gopalan and Margolin (1991), Hu *et al*. (1996), Hu and Wang (1997a,b,c, 1998a,b), Peralta and Laird (1997, 1998), Zhang and Wang (1998a,b,c, 1999) and Zhang *et al*. (1998, 1999a,b). In the previous studies of the bicrystals, some open questions remained. For example, all the large-angle GBs in the bicrystals studied previously always acted as obstacles against the PSBs passing through, because there was no common primary slip plane belonging to the two component crystals. As a result, dislocations or PSBs could not pass through the large-angle GBs (Hu and Wang 1997a,b, Zhang and Wang 1998a, 1999) and, therefore, dislocations often piled up at them. Furthermore, fatigue cracks prefer to nucleate along GBs, irrespective of whether the GB is perpendicular to, parallel to or inclined at an angle to the stress axis (Peralta and Laird 1997, 1998, Hu and Wang 1997a,b, 1998a, Zhang *et al*. 1998, 1999a,b). Recently, it was found that both the surface PSBs and dislocations can pass through small-angle GBs perfectly, because the adjacent grains possess nearly the same slip planes and slip directions in copper columnar crystals (Zhang and Wang 1998a). In the present work, we have grown a copper bicrystal for which two component crystals contain a common primary slip plane, in the expectation that the PSBs and dislocations can transfer through the GB continuously, as with small-angle GBs.

The scanning electron microscopy (SEM) electron channelling contrast (ECC) technique has been successfully applied to study the dislocation patterns in deformed metals such as stainless steel (Zauter *et al*. 1992), nickel (Schwab *et al* 1996, 1998), copper (Gong *et al*. 1997, Melisova *et al*. 1997, Li *et al*. 1998, Jia *et al*. 1999) and aluminium (Mitchell and Day 1998). The SEM ECC technique not only reveals information difficult to achieve by the conventional transmission electron microscopy technique but also allows the observations of dislocation patterns over the whole cross-section of the specimen, and the dislocations in some special sites can also be revealed, for example in the vicinity of GBs (Zhang and Wang 1998a, 1999), deformation bands (Gong *et al*. 1997, Li *et al*. 1998) and ahead of a crack (Ahmed *et al*. 1997, Jia *et al*. 1999). Therefore, in the present paper, the SEM ECC technique has been utilized to reveal the cyclic stress–strain (CSS) response and the interactions between dislocations, PSBs and the GB in the copper bicrystal.

§ 2. Experimental procedure

A bicrystal of size 150 mm × 50 mm × 10 mm was grown from OFHC copper of 99.999% purity by the Bridgman method. By the electron back-scattering diffraction (EBSD) technique, it was found that the rotation angle of the two grains is 46.2° in the [111] axes. To investigate the fatigue behaviour of the copper bicrystal with a common primary slip plane, a group of fatigue specimens with gauge dimensions of 6 mm × 6 mm × 16 mm and a GB plane inclined to the tensile axis were designed.

The orientations of the two component grains in the bicrystal were determined as follows:

$$\mathbf{G}_1 = \begin{bmatrix} -0.6456 & 0.1551 & -0.7477 \\ 0.5498 & -0.5851 & -0.5961 \\ -0.5300 & -0.7960 & 0.2924 \end{bmatrix} = \begin{bmatrix} -13 & 4 & -5 \\ 11 & -15 & -4 \\ -11 & -20 & 2 \end{bmatrix},$$

$$\mathbf{G}_2 = \begin{bmatrix} -0.3576 & 0.9211 & 0.1540 \\ 0.1540 & -0.1045 & -0.9825 \\ 0.9211 & 0.3750 & -0.1045 \end{bmatrix} = \begin{bmatrix} -12 & 18 & 3 \\ 5 & -2 & 20 \\ 30 & 7 & -2 \end{bmatrix}.$$

In brief, the axis orientations of the two grains are typical for single slip and can be referred to as $\mathbf{G}_1[\bar{4}\,15\,20]$ and $\mathbf{G}_2[18\,\bar{2}\,7]$ respectively. The Schmid factors of the common primary slip systems are nearly the same and equal to 0.47 ($\Omega_{\mathbf{G}_1}$) and 0.49 ($\Omega_{\mathbf{G}_2}$) respectively. The crystallographic relationship of the bicrystal is shown in figure 1, where it can be seen that the primary slip planes of the two grains are coplanar.

Before cyclic deformation, all the bicrystal specimens were electropolished carefully for surface observation. Cyclic push–pull tests were performed on a Shimadzu servohydraulic testing machine under constant-plastic-strain control at room temperature in air. A triangle waveform with a frequency range 0.1–0.3 Hz was used.

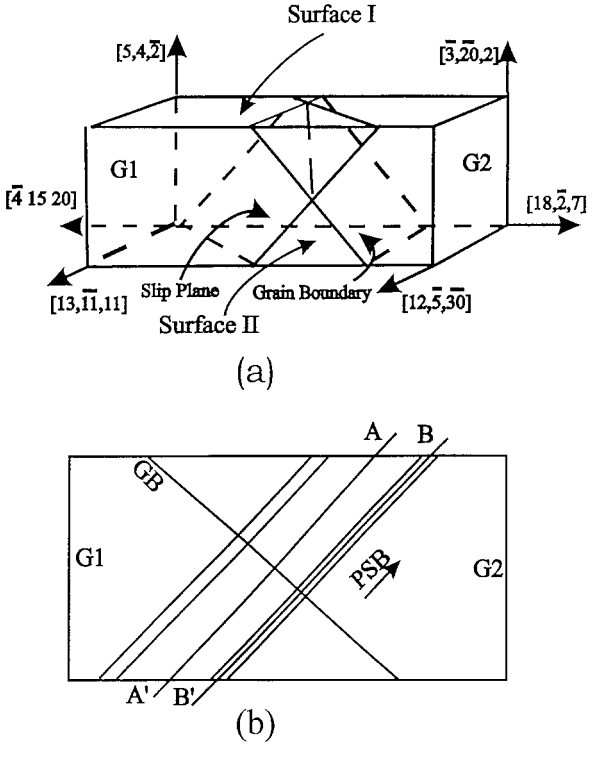

Figure 1. (*a*) Crystallographic relationship between primary slip plane and GB in the bicrystal; (*b*) sectioning procedure along primary slip plane of the bicrystal.

Table 1. The working conditions of the SEM ECC technique.

Acceleration voltage (kV)	Working distance (mm)	Filament current (A)	Probe current (A)	Brightness (%)	Contrast (%)	Scanning rate
20	15–20	2–3	2–5	60–75	30–33	TV/2K

The peak loads in tension and compression were recorded continuously, and the hysteresis loops were recorded at intervals on an X-Y recorder until cyclic saturation occurred. The applied axial plastic strain amplitudes $\Delta\varepsilon_{pl}/2$ were in the range 1.5×10^{-4}-2.13×10^{-3}. After cyclic saturation, the slip morphology on the bicrystal surfaces was examined. Then, the fatigued bicrystals were polished again to remove the slip traces. The dislocation patterns on the surfaces within grains and near the GB were observed by the SEM ECC technique in a Cambridge S360 scanning electron microscope. Similar to the image system reported by Schwab *et al.* (1996), an inverted imaging mode was adopted in the present investigation. Thus, the bright areas in the ECC micrograph represent regions of low dislocation density, whereas the dark areas represent dislocation-dense regions, which are in accord with the transmission electron micrograph under bright imaging conditions. The parameters of the SEM working conditions are listed in table 1. In addition, some fatigued bicrystal specimens were sectioned along the common primary slip plane to reveal the interactions of PSBs with the GB by this technique. The section process is illustrated in figure 1 (*b*). Then, the sectioned surface was repeatedly polished to examine the dislocation patterns at different depths.

§ 3. Experimental results

3.1. *Cyclic stress–strain response*

The cyclic hardening curves at different strain amplitudes are shown in figure 2 (*a*), where the axial stress amplitude is plotted. Similar to the results of copper single crystals (Mughrabi 1978), the initial cyclic hardening rate of the bicrystal also increases with increasing plastic strain amplitude. With further cyclic deformation, all the bicrystals exhibit a saturation behaviour with nearly the same axial saturation stresses of 61.6–63.5 MPa in the axial plastic strain range 1.5×10^{-4}-2.13×10^{-3}. The CSS curves plotted as axial saturation stress versus axial plastic strain amplitude are illustrated in figure 2 (*b*). For comparison, the CSS curves of [$\bar{5}$ 9 13]–[$\bar{5}$79] and [$\bar{1}$34]-[$\bar{1}$34] copper bicrystals are also included in the figure. It can be seen that the CSS curve of the [$\bar{4}$ 15 20]–[18 $\bar{2}$ 7] copper bicrystal displays a very long plateau region in the axial plastic strain range 1.5×10^{-4}-2.13×10^{-3}. This feature is very close to those of the copper single crystal (Mughrabi 1978, Cheng and Laird, 1981) and [$\bar{1}$34]–[$\bar{1}$34] copper bicrystals (Hu and Wang 1998b). For a [$\bar{5}$ 9 13]–[$\bar{5}$79] copper bicrystal, the CSS curve displays two distinct plateau regions, but the strain range is relatively short (Zhang and Wang 1999). The saturation stresses of the [$\bar{4}$ 15 20]–[18 $\bar{2}$ 7], [$\bar{5}$ 9 13]-[$\bar{5}$79] and [$\bar{1}$34]–[$\bar{1}$34] copper bicrystals are listed in table 2. Apparently, the axial saturation stresses of the [$\bar{4}$ 15 20]–[18 $\bar{2}$ 7] and [$\bar{1}$34]–[$\bar{1}$34] bicrystals are basically equal to those in lower plateau region of the [$\bar{5}$ 9 13]–[$\bar{5}$79] bicrystal.

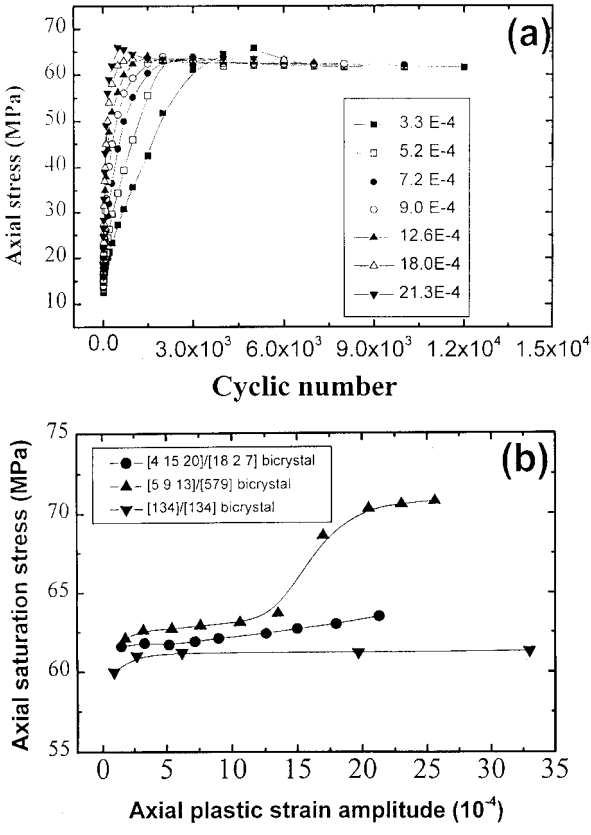

Figure 2. (*a*) Cyclic hardening curves of the $[\bar{4}\,15\,20]$–$[18\,\bar{2}\,7]$ copper bicrystal at different strain amplitudes; (*b*) CSS curves of $[\bar{4}\,15\,20]$–$[18\,\bar{2}\,7]$, $[\bar{1}34]$–$[134]$ and $[\bar{5}\,9\,13]$–$[\bar{5}\,7\,9]$ copper bicrystals.

Using the Schmid law and the data in table 2, the saturation resolved shear stresses $\tau_{\mathbf{G}_1}$ and $\tau_{\mathbf{G}_2}$ of the crystals $\mathbf{G}_1$ and $\mathbf{G}_2$ can be calculated from the following equations:

$$\tau_{\mathbf{G}_1} = \sigma_B \Omega_{\mathbf{G}_1}, \tag{1}$$

$$\tau_{\mathbf{G}_2} = \sigma_B \Omega_{\mathbf{G}_2}, \tag{2}$$

where σ_B is the axial saturation stress amplitude of the bicrystal. The calculated results for $\tau_{\mathbf{G}_1}$ and $\tau_{\mathbf{G}_2}$ are also listed in table 2 and are equal to 28.9–29.8 and 30.2–31.1 MPa respectively, which is approximately equal to the plateau saturation resolved shear stress (28–30 MPa) of the copper single crystal oriented for single slip (Mughrabi 1978, Cheng and Laird 1981). Similarly, the resolved shear stresses of each component grain in $[\bar{5}\,9\,13]$–$[\bar{5}79]$ and $[\bar{1}34]$–$[\bar{1}34]$ copper bicrystals can also be calculated from equations (1) and (2) and are listed in table 2. It is indicated that the saturation resolved shear stresses of those bicrystals are very close to that of copper single crystals and are not affected by the GB, which will be discussed in the following sections.

Table 2. Saturation stresses of $[\bar{4}\,15\,20]$–$[18\,\bar{2}\,7]$, $[\bar{1}34]$–$[\bar{1}34]$ and $[\bar{5}\,9\,13]$–$[\bar{5}79]$ copper bicrystals.

$[\bar{4}\,15\,20]$–$[18\,\bar{2}\,7]$ bicrystal				$[\bar{1}34]$–$[134]$ bicrystal			$[\bar{5}\,9\,13]$–$[\bar{5}79]$ bicrystal			
ε_{pl} $\times 10^{-4}$	$\sigma_{[\bar{4}\,15\,20]-[18\,\bar{2}\,7]}$ (MPa)	$\tau_{[\bar{4}\,15\,20]}$ (MPa)	$\tau_{[18\,\bar{2}\,7]}$ (MPa)	ε_{pl} $\times 10^{-4}$	$\tau_{[\bar{1}34]-[\bar{1}34]}$ (MPa)	$\tau_{[\bar{1}34]}$ (MPa)	ε_{pl} $\times 10^{-4}$	$\sigma_{[\bar{5}\,9\,13]-[\bar{5}79]}$ (MPa)	$\tau_{[\bar{5}\,9\,13]}$ (MPa)	$\tau_{[\bar{5}79]}$ (MPa)
1.5	61.6	28.9	30.2	0.9	60.0	28.2	1.8	62.1	28.1	25.3
3.3	61.8	29.0	30.3	2.7	61.0	28.7	3.2	62.6	28.3	25.5
5.2	61.7	29.0	30.3	6.2	61.2	28.8	5.4	62.7	28.3	25.5
7.2	61.9	29.1	30.4	19.7	61.2	28.8	7.6	62.9	28.4	25.6
9.0	62.1	29.2	30.5	33.0	61.3	28.8	10.6	63.1	28.5	25.7
12.6	62.4	29.3	30.6	—	—	—	13.5	63.7	28.8	25.9
15.0	62.7	29.5	30.7	—	—	—	17.0	68.6	31.0	27.9
18.0	63.0	29.6	30.9	—	—	—	20.5	70.3	31.8	28.5
21.3	63.5	29.8	31.1	—	—	—	23.0	70.6	31.9	32.0
—	—	—	—	—	—	—	25.6	70.8	32.0	28.8

3.2. *Surface slip morphology*

SEM and optical microscopy observations revealed that the surface slip morphologies of the cyclically saturated copper bicrystals at different strain amplitudes displayed the following features. On both $\mathbf{G}_1$ and $\mathbf{G}_2$ grains, as expected, the common primary slip bands were activated on the whole surface, including in the vicinity of the GB. This slip feature is consistent with that of the single-slip-oriented copper single crystals. Figure 3 (*a*) gives the slip morphology near the GB on surface I. It is worth noting that those slip bands have a good one-to-one relationship across the GB, but secondary slip bands cannot be seen. When observing surface II of the bicrystal, the one-to-one relationship of slip bands within $\mathbf{G}_1$ and $\mathbf{G}_2$ grains can also be seen, as shown in figure 3 (*b*). It follows that common primary slip bands transferred through the GB continuously during cyclic deformation on the four surfaces of the bicrystal.

With increasing strain amplitude or cycle number, plastic strain incompatibility near the GB might occur. Figure 4 (*a*) shows that secondary slip bands or deformation bands (DBs) seem to occur near the GB surface II. However, a clearer micrograph indicates that secondary slip bands or DBs were not activated, as shown in

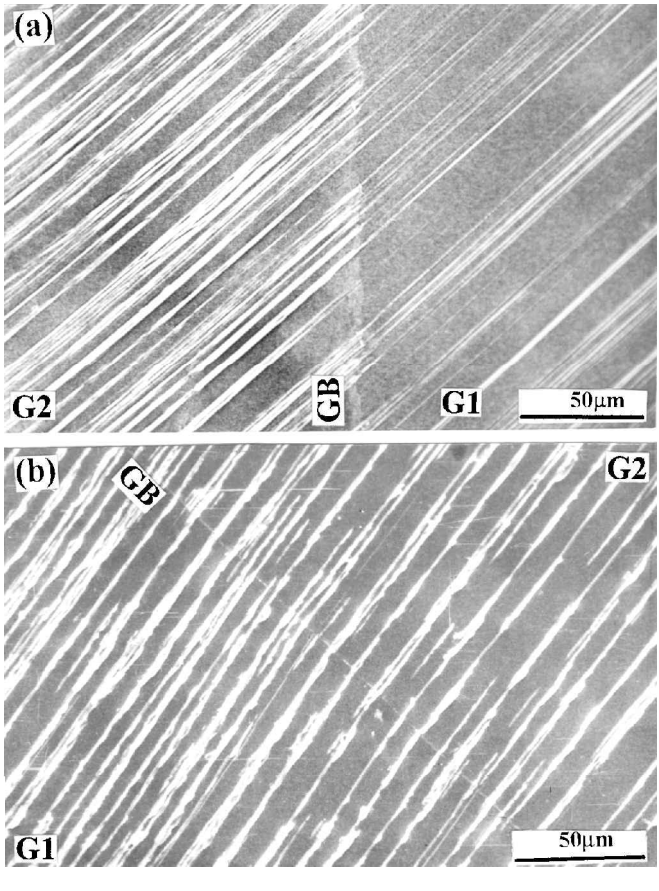

Figure 3. Slip morphology near the GB on (*a*) surface I of the bicrystal and (*b*) surface II of the bicrystal.

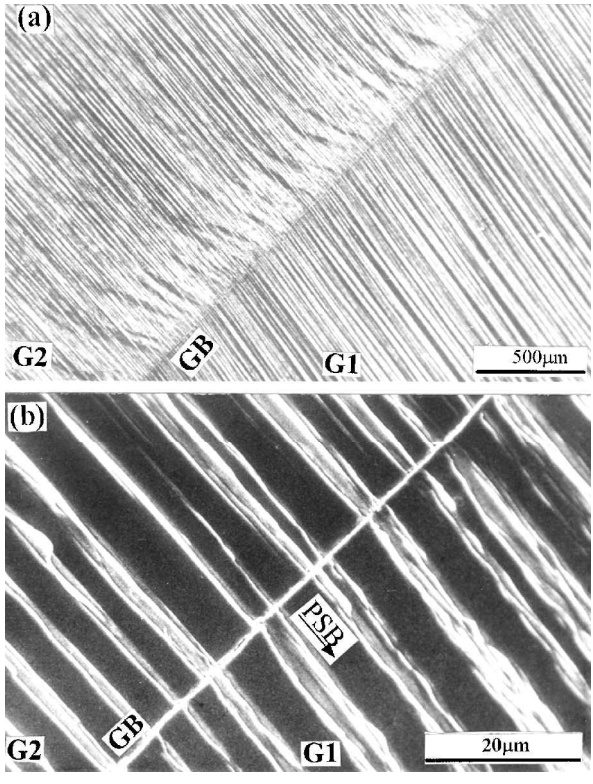

Figure 4. Slip morphology near the GB on surface II of the bicrystal cyclically deformed at a higher strain amplitude ($\varepsilon_{pl} = 1.8 \times 10^{-3}$): (*a*) at a low magnification; (*b*) at a high magnification.

figure 4 (*b*). Those observations indicate that surface slip bands can transfer through the GB of the fatigued copper bicrystals with common primary slip planes, while some plastic strain incompatibility near the GB may still occur at higher strain amplitudes or higher cycles.

3.3. *Dislocation pattern observations*

By the SEM ECC technique, the ladder-like PSBs and dislocation veins can be observed on both surfaces within the $\mathbf{G}_1$ grain of the bicrystal, as shown in figure 5 (*a*). These dislocation patterns are in good agreement with the two-phase structure in copper single crystals (Winter 1974, Finney and Laird 1975, Laird *et al.* 1986). However, for the $\mathbf{G}_2$ grain, the ladder-like PSBs only appear on surface I and, instead, the dislocations consist of irregular veins on surface II, as shown in figure 5 (*b*). This difference is reasonable, since the primary slip directions of the $\mathbf{G}_1$ and $\mathbf{G}_2$ grains are obviously different owing to the misorientation. This is in contrast with observations on $[\bar{5}\,9\,13]$–$[\bar{5}79]$ copper bicrystals, in which the ladder-like PSBs were not observed simultaneously within the two grains (Zhang and Wang 1999). At low strain amplitudes, the ladder-like PSBs mainly formed in the softer $[\bar{5}\,9\,13]$ grain, while the dislocation patterns only consisted of irregular veins in the harder $[\bar{5}79]$ grain. At higher strain amplitudes, the ladder-like PSBs began to form in the harder

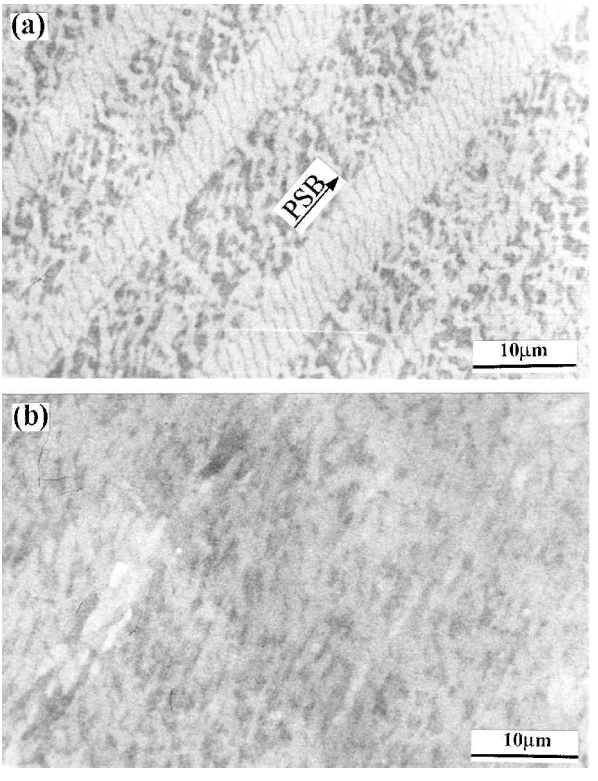

Figure 5. (*a*) Typical two-phase structure of PSBs and veins within $\mathbf{G}_1$ and $\mathbf{G}_2$ grains; (*b*) irregular dislocation arrangements within a $\mathbf{G}_2$ grain on surface II.

[$\bar{5}$79] grain; in this case, the softer [$\bar{5}$ 9 13] contained parallel dislocation walls or a labyrinth. In addition, for [$\bar{3}$45]–[$\bar{1}$17] copper bicrystals, ladder-like PSBs were seldom found. Instead, dislocation cells, veins or a labyrinth are very common (Hu and Wang 1997c). This is because [$\bar{3}$45] and [$\bar{1}$17] grains are close to the [$\bar{1}$11] and [001] multislip orientations, whereas [$\bar{5}$ 9 13] and [$\bar{5}$79] grains orient for typical single slip. It follows that the saturation dislocation patterns within grains in the bicrystals above strongly depend on the crystal orientations like that in copper single crystals.

The dislocation arrangements near the GB at different surfaces of the specimen reveal two kinds of feature. On surface I of the bicrystal, the dislocation walls carried by ladder-like PSBs are also continuous and regular beside the GB, as shown in figure 6 (*a*). This result indicates that the ladder-like PSBs can also transfer through the large-angle GB continuously on this surface and are highly consistent with the surface slip bands near the GB (figure 3 (*a*)). This feature is similar to that beside the small-angle GBs in fatigued copper columnar crystals (Zhang and Wang 1998a). When observing surface II of the bicrystal, it seems that the ladder-like PSBs beside the GB also have a one-to-one relationship at low magnifications, as shown in figure 6 (*b*). However, at higher magnifications, it can be clearly seen that the ladder-like PSBs within the $\mathbf{G}_1$ grain can reach the GB but become rather irregular within the $\mathbf{G}_2$ grain, as shown in figure 6 (*c*). In particular, the ladder-like PSBs in the $\mathbf{G}_1$ grain seem to produce an affected zone near the GB in the adjacent $\mathbf{G}_2$ grain. If the cycle number is increased, the PSBs interact more strongly with the GB, as shown in figure

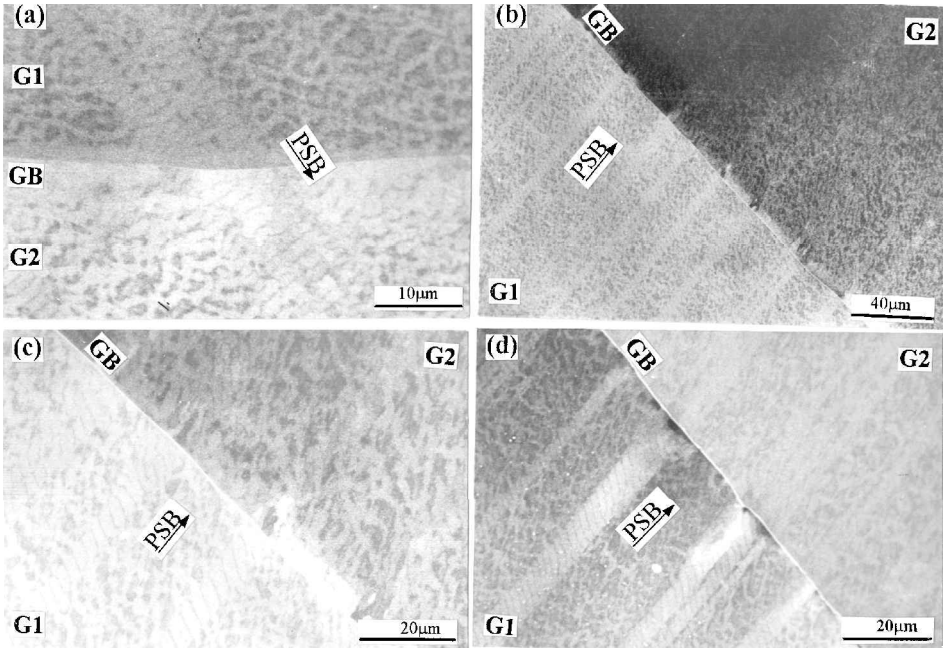

Figure 6. (*a*) Dislocation pattern near the GB on surface I ($\varepsilon_{pl} = 12.6 \times 10^{-4}$; $N = 7 \times 10^4$ cycles); (*b*)–(*d*) dislocation patterns near the GB on surface II (*b*) at $\varepsilon_{pl} = 9 \times 10^{-4}$, $N = 10^4$ cycles and a low magnification, (*c*) at $\varepsilon_{pl} = 9 \times 10^{-4}$, $N = 10^4$ cycles and a high magnification and (*d*) at $\varepsilon_{pl} = 10^{-3}$ and $N = 2 \times 10^4$.

6 (*d*). Those observations are not consistent with the surface slip bands in figure 3 (*b*), indicating that the ladder-like PSBs could not completely transfer through the GB over the whole specimen despite the fact that the two grains in the bicrystal have a common primary slip plane.

When observing the dislocation arrangements near the GB on the (111) plane after polishing, it is found that not all the dislocation veins can reach the GB, as shown in figure 7 (*a*) and that a dislocation-affected zone (DAZ) appears. The DAZ is about 5–10 μm in width and only appears at one side of the GB. In appearance, it is very similar to the dislocation-free zone (DFZ) observed in $[\bar{3}45]$–$[\bar{1}17]$ and $[\bar{1}35]$–$[\bar{1}35]$ copper bicrystals and polycrystals (Hu and Wang 1997c, 1998a, Winter *et al.* 1981, Luoh and Chang 1996), but there is some difference between the DAZ and the so-called DFZ. First, the width (5–10 μm) of the DAZ is about five times the width (1–2 μm) of the DFZ; second, at high magnifications, there are still some dislocations within the DAZ, as shown in figure 7 (*b*), indicating that the DAZ is not dislocation free. It is suggested that the formation of a DAZ or a DFZ near the GB might be a common phenomenon in fatigued copper bicrystals and polycrystals. Essentially, it might be the same structure induced by the interactions between dislocations and GBs. The above difference might be attributed to differences in observed plane. It is found that the DAZ near the GB can also form within the $\mathbf{G}_2$ grain, as shown in figure 7 (*c*). The widths of the DAZ within the two grains far from the specimen centre are nearly the same (5–10 μm). However, close to the specimen centre, the DAZ near the GB gradually disappears, as shown in figure 7 (*d*).

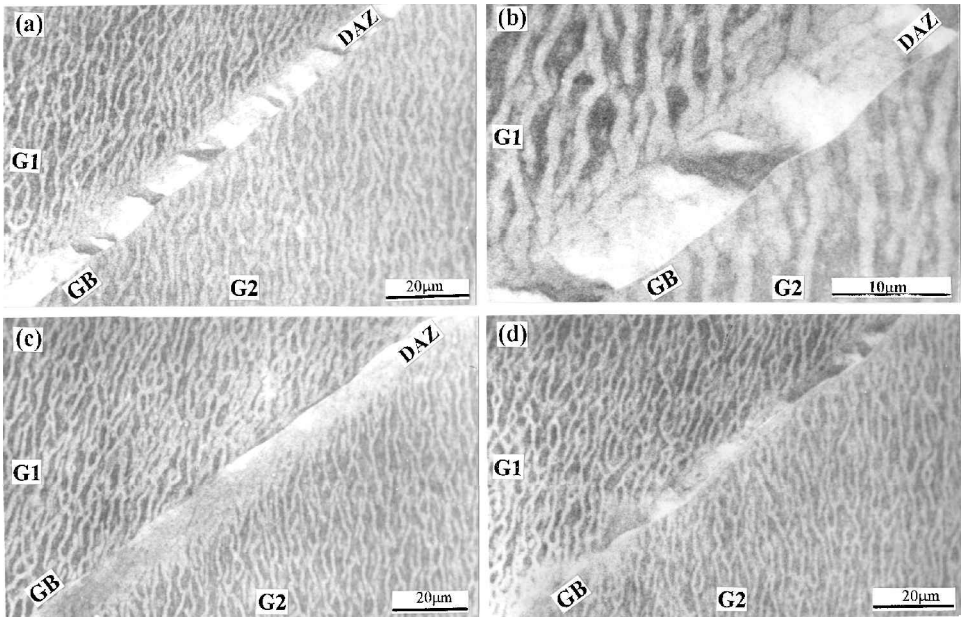

Figure 7. DAZ, near the GB on the common primary slip plane of the bicrystal ($\varepsilon_{pl} = 9 \times 10^{-4}$; $N = 10^4$): (*a*), (*b*) DAZ within the $\mathbf{G}_1$ grain (*a*) at a low amplitude and (*b*) at a higher magnification; (*c*) DAZ within the $\mathbf{G}_2$ grain; (*d*) irregular DAZ in the centre of the GB.

The above-mentioned interactions of dislocations with the GB might mainly correspond to the A–A′ layer in figure 1 (*b*). When the observation surface lies in the B–B′ layer in figure 1 (*b*), PSB walls will be seen on the common primary slip plane. In this case, it is found that the dislocation walls can also reach or be close to the GB. There are, however, still several kinds of interaction mode between PSB walls and the GB in the bicrystal. Figure 8 (*a*) shows that the PSB walls within the $\mathbf{G}_1$ grain reach the GB, and the DAZ does not nucleate between the dislocation walls and the GB. By contrast, within the adjacent $\mathbf{G}_2$ grain, there is still a DAZ with a width of 5–10 μm near the GB. Another interesting finding is that the DAZ can also nucleate between the PSB walls and the GB, as shown in figure 8 (*b*). The width of the DAZ between the GB and PSB walls, in this case, is also equal to 5–10 μm. This indicates that the PSB walls do not affect the formation of the DAZ. Observations layer by layer on the plane show that almost all the PSB walls within the two grains do not have a one-to-one correlation across the GB. Occasionally, the PSBs within the two grains may intersect on the same site of the GB, as shown in figures 8 (*c*) and (*d*). In this special case, the PSBs often become bent or discontinuous as they are close to the GB. The dislocation walls in the PSBs are still straight and can be clearly distinguished even though they may disappear or become veins in some local regions. It is noted that there seems to be a strong interaction between the GB and the PSB walls. The reason could be that most of plastic strain is localized in the PSB walls during cyclic deformation, especially when the two PSBs within the $\mathbf{G}_1$ and $\mathbf{G}_2$ grains intersect on the same side of the GB. This could explain why the PSBs became bent or discontinuous as they reached the GB. Based on the observations above, the typical interaction modes between PSBs and the GB on the common primary slip

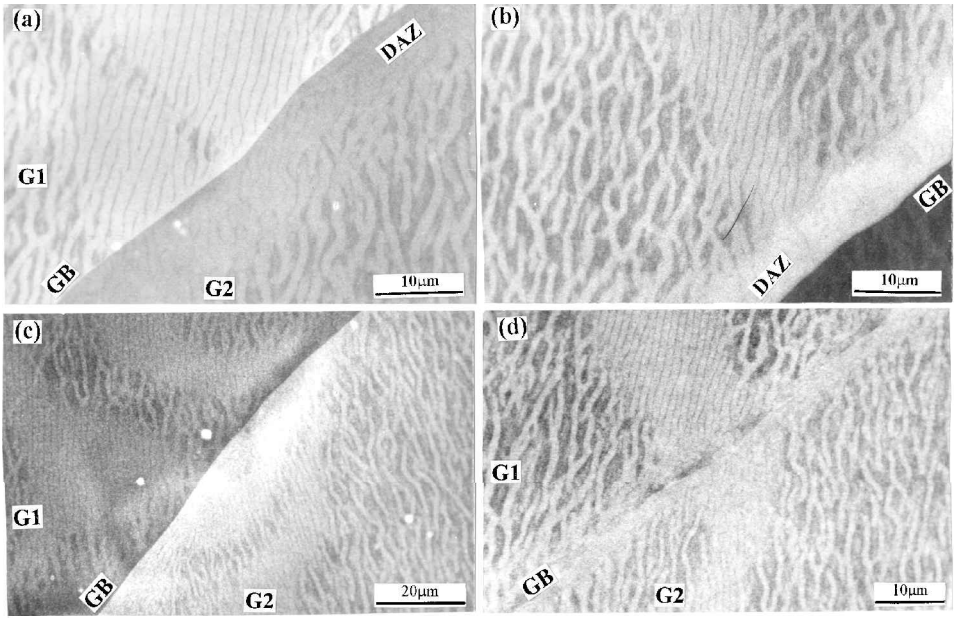

Figure 8. Different kinds of interaction and dislocations, PSBs and the GB.

plane can be illustrated schematically as in figure 9 (*a*). It is suggested that the dislocations in PSBs cannot pass through the GB continuously even though the two grains have a common primary slip plane.

§ 4. Discussion

4.1. *Interactions between dislocations, persistent slip bands and the grain boundary*

During the past decade, several researchers have investigated the interactions between dislocations, slip bands and GBs. The results show that dislocations are often piled up at the GBs owing to the difference in the slip systems between adjacent grains. When dislocations meet a GB, they will firstly be transferred directly through the GB into the adjoining grain, secondly be absorbed and transformed into extrinsic GB dislocations, thirdly be accommodated in the GB, followed by the emission from the GB of a matrix dislocation, and, fourthly, be ejected back into their original grain. To predict which slip system is favourable for slip transfer, three criteria have been proposed (Lim 1984, Lim and Raj 1985a,b, Shen *et al.* 1986, Lee *et al.* 1989, 1990). First, the angle between the lines of interaction of incoming and outgoing slip planes with the GB should be as small as possible. Second, the resolved shear stress acting on the possible slip systems in the adjoining grain should be large. Third, the magnitude of the Burgers vector of the extrinsic dislocations left at the GB following emission of dislocation should be a minimum.

The criteria above might be necessary for slip transferring through a GB under monotonic loading. However, under cyclic loading, it is not clear what kinds of GB can be passed through by the dislocations and PSBs. Recent studies on copper bicrystals with large-angle GBs showed that all the surface slip bands (or PSBs) terminated at the GB after cyclic deformation of those bicrystals. Further micro-

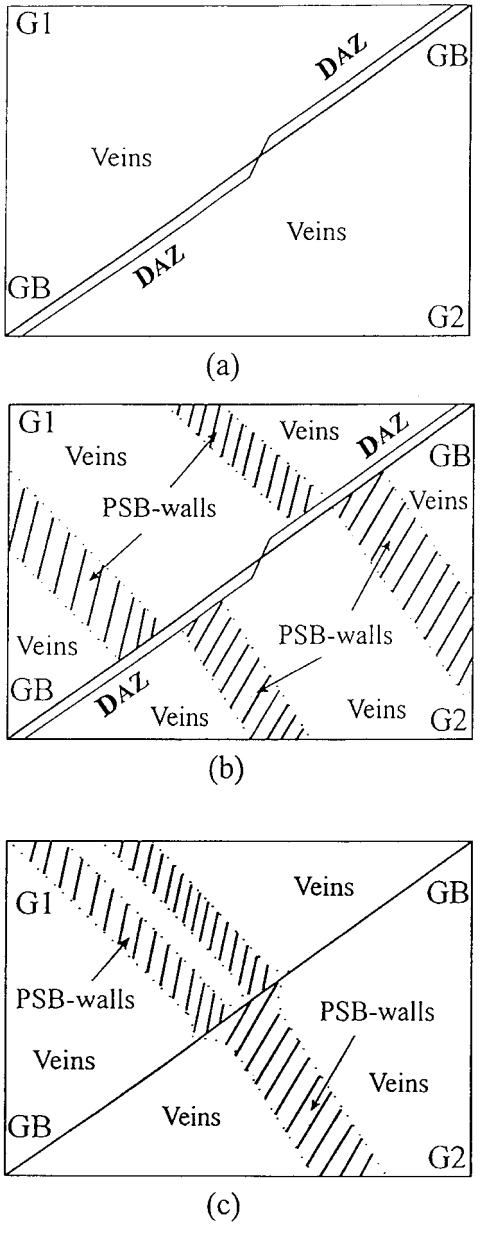

Figure 9. Sketches of the interactions between dislocations, PSBs and the GB.

scopic observations show that the dislocation arrangements beside the GB are also discontinuous; sometimes, DFZs form near the GB in [$\bar{3}$45]–[$\bar{1}$17] and [$\bar{1}$35]–[$\bar{1}$35] copper bicrystals (Hu and Wang 1997a,b,c). In a [$\bar{5}$ 9 13]–[$\bar{5}$79] copper bicrystal, it was observed that the PSBs within the [$\bar{5}$ 9 13] grain can extend to the GB with a sharp end and produce some affected zones in the neighbouring [$\bar{5}$79] grain. Those affected zones developed along a direction other than the primary slip direction of the [$\bar{5}$79] grain (Zhang and Wang 1998a, 1999). Based on the previous investigations,

it can be concluded that, in fact, dislocations or PSBs transfer only with difficulty through a large-angle GB under cyclic loading because the primary slip planes of adjacent grains are seldom coplanar. More recently, it was observed that both dislocations and PSBs can transfer through small-angle GBs completely in a copper columnar crystal (Zhang and Wang 1998a) and subgrain boundaries (Winter *et al.* 1981). The interactions between dislocations, PSBs and small-angle GBs can be schematically illustrated as in figure 10 (*a*). Obviously, the PSBs in neighbouring grains are coplanar so that the surface PSBs and dislocations can easily pass through small-angle GBs, irrespective of whether they are parallel or perpendicular to the stress axis. In particular, the Burgers vectors of those adjacent grains on the common slip plane are nearly the same so that the dislocation walls beside the small-angle GB will be parallel to each other. Obviously, this geometrical relation is the most favourable condition for slip transfer according the criteria summarized above (Lim 1984, Lim and Raj 1985a,b, Shen *et al.* 1986, Lee *et al.* 1989, 1990).

For the present bicrystal, by crystallographic analysis, it is found that the Burgers vectors $\mathbf{b}_1$ and $\mathbf{b}_2$ of the $\mathbf{G}_1$ and $\mathbf{G}_2$ grains have an interaction angle θ (about 13.8°) on the common primary slip planes, as shown in figure 9. This results in the difference in the directions of dislocation walls beside the GB on the common slip plane, as shown in figure 10 (*b*). Therefore, the discontinuous ladder-like PSBs on surface II can be attributed to the misorientation between the $\mathbf{G}_1$ and $\mathbf{G}_2$ grains, as well as the different kinds of interaction between dislocations, PSBs and the GB (figures 6–9). It is suggested that the PSBs could only partially transfer through the GB during cyclic deformation of the bicrystals. Furthermore, we can conclude that it is more difficult for slip to transfer through a large-angle GB under cyclic loading than under monotonic loading.

4.2. *Effect of component crystal orientations on the cyclic stress-strain curves of copper bicrystals*

The cyclic deformation behaviour of a bicrystal containing two component grains and a GB should depend on the component crystal orientations and the GB type. Generally, the GB can be perpendicular, parallel or inclined to the stress axis in a bicrystal. For the first case, such as [$\bar{3}$45]–[$\bar{1}$17], [$\bar{1}$34]–[$\bar{1}$34], [$\bar{5}$ 9 13]–[$\bar{5}$79] and [$\bar{1}$23]–[$\bar{3}$35] copper bicrystals, it is found that their CSS curves depend strongly on the orientations of the two component grains (Zhang and Wang 1998b). At low strain amplitudes, the softer grains with a relatively higher Schmid factor influence

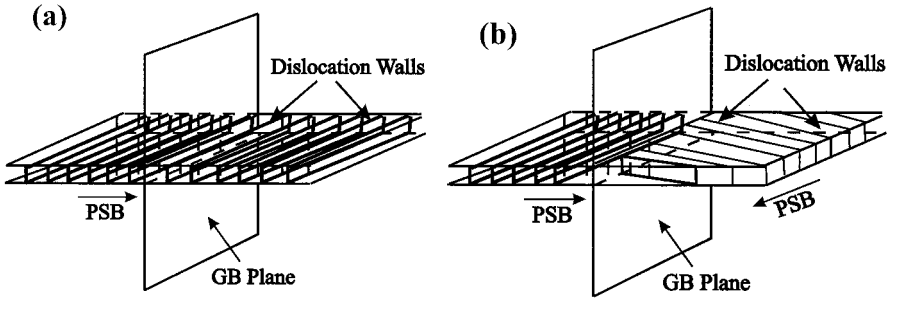

Figure 10. Sketches of the interactions between dislocations and different kinds of GB: (*a*) continuous dislocations beside a small-angle GB; (*b*) discontinuous dislocations beside the $\Sigma = 19$ GB.

mainly the saturation stresses of the bicrystals. With increasing strain amplitude, the harder grains with a relatively lower Schmid factor may play a decisive role in the saturation stresses of the bicrystals. Therefore, the distribution of plastic strain in a bicrystal with a perpendicular GB is

$$\varepsilon_{\mathrm{B}} = \frac{\varepsilon_{\mathbf{G}_1} + \varepsilon_{\mathbf{G}_2}}{2}. \tag{3}$$

Here ε_{B}, $\varepsilon_{\mathbf{G}_1}$ and $\varepsilon_{\mathbf{G}_2}$ are the mean plastic strains carried by the bicrystal, and grains $\mathbf{G}_1$ and $\mathbf{G}_2$ respectively. If the grain $\mathbf{G}_1$ is softer than grain $\mathbf{G}_2$ in a bicrystal, we obtain

$$\varepsilon_{\mathbf{G}_1} > \varepsilon_{\mathrm{B}} > \varepsilon_{\mathbf{G}_2}. \tag{4}$$

This means that the saturation will be affected by the orientations of two component grains. Consequently, the CSS curves of the copper bicrystals mentioned above display different plateau regions.

On the other hand, when the GB is parallel to the loading direction, as in [$\bar{1}$35]–[$\bar{1}$35], [$\bar{1}$35]–[$\bar{2}$35], [$\bar{2}$35]–[$\bar{2}$35] and [$\bar{6}$79]–[$\bar{1}$45] copper bicrystals (Hu *et al*. 1996, Zhang and Wang 1998a), their saturation stresses can be given as

$$\begin{aligned}\sigma_{\mathrm{B}} &= \sigma_{\mathbf{G}_1} \mathrm{V}_{\mathbf{G}_1} + \sigma_{\mathbf{G}_2} \mathrm{V}_{\mathbf{G}_2} + \sigma_{\mathrm{GB}} \\ &= \tau_{\mathrm{PSB}} \left(\frac{\mathrm{V}_{\mathbf{G}_1}}{\Omega_{\mathbf{G}_1}} + \frac{\mathrm{V}_{\mathbf{G}_2}}{\Omega_{\mathbf{G}_2}} \right) + \sigma_{\mathrm{GB}}.\end{aligned} \tag{5}$$

Here, σ_{B} $\sigma_{\mathbf{G}_1}$ and $\sigma_{\mathbf{G}_2}$ are the mean axial saturation stresses carried by the bicrystal, the $\mathbf{G}_1$ grain and the $\mathbf{G}_2$ grain respectively. σ_{GB} can be regarded as an additional stress caused by the GB owing to the plastic strain incompatibility. τ_{PSB} represents the stress activating PSBs and is equal to 28–30 MPa for single-slip-oriented copper single crystals (Mughrabi, 1978, Cheng and Laird 1981). $\mathrm{V}_{\mathbf{G}_1}$ and $\mathrm{V}_{\mathbf{G}_2}$ are the volume fractions of the $\mathbf{G}_1$ and $\mathbf{G}_2$ grains respectively. $\Omega_{\mathbf{G}_1}$ and $\Omega_{\mathbf{G}_2}$ are the Schmid factors of the primary slip systems of the $\mathbf{G}_1$ and $\mathbf{G}_2$ grain respectively. In equation (5), τ_{PSB}, $\mathrm{V}_{\mathbf{G}_1}$ and $\mathrm{V}_{\mathbf{G}_2}$ are constants for a given bicrystal. Thus, the saturation stress of the bicrystal will depend on the orientations (or $\Omega_{\mathbf{G}_1}$ and $\Omega_{\mathbf{G}_2}$) of the $\mathbf{G}_1$ and $\mathbf{G}_2$ grains as well as the additional stress σ_{GB} induced by the GB. This indicates that the saturation stress of the bicrystal with a parallel GB will be increased if the $\mathbf{G}_1$ and $\mathbf{G}_2$ grains have lower Schmid factors.

The present bicrystal with a tilted GB belongs to the third type. In particular, its component grains contain a common primary slip plane, which transfers through the GB continuously, as observed above. During cyclic deformation, the plastic strain of the bicrystal will be localized on the common primary slip bands. It is known that the Schmid factors of the $\mathbf{G}_1$ and $\mathbf{G}_2$ grains are equal to 0.47 ($\Omega_{\mathbf{G}_1}$) and 0.49 ($\Omega_{\mathbf{G}_2}$), and τ_{PSB} is equal to 28–30 MPa. Substituting $\Omega_{\mathbf{G}_1}$, $\Omega_{\mathbf{G}_2}$ and τ_{PSB} into equations (1) and (2), the axial saturation stresses of the $\mathbf{G}_1$ and $\mathbf{G}_2$ grains should be in the range 59.6–63.8 and 57.1–61.2 MPs respectively. From the experimental results in table 2, the axial saturation stresses of the bicrystal are in the range 61.2–63.5 MPa, that is very close to those of the grain $\mathbf{G}_1$ and the grain $\mathbf{G}_2$. Therefore, the long plateau region in the CSS curve of the bicrystal can be attributed to the following reasons. The first is that the two grains are oriented for typical single slip and, in particular, their Schmid factors are nearly the same. The second is that the primary slip planes of the $\mathbf{G}_1$ and $\mathbf{G}_2$ grains are coplanar and the common PSBs can transfer through the GB con-

tinuously. The last reason, which might be the most important, is that the GB did not play a strengthening role in the bicrystal, when the common PSBs passed through the GB. The observations on slip morphology and dislocation patterns indicate that the GB actually plays a small strengthening role in the bicrystal like the small-angle GBs in a copper columnar crystal (Zhang and Wang 1998a). As a result, we can consider the bicrystal as a single crystal if only the stress distribution is taken into account. Meanwhile, it has been observed that the ladder-like PSBs can nucleate within the $\mathbf{G}_1$ and $\mathbf{G}_2$ grains simultaneously. Consequently, the two-phase model proposed by Winter (1974) and Finney and Laird (1975) can be applied to the present special bicrystal, indicating that a common PSB across the GB in the bicrystal can be regarded like a single PSB in a single crystal and that the PSBs carry most of the plastic strain during cyclic deformation.

§ 5. Conclusions

(1) The CSS curve of the present copper bicrystal displays a distinct plateau region with an axial saturation stress of 61.6–63.5 MPa over the axial plastic strain range from 1.5×10^{-4} to 2.13×10^{-3}. If modified by the Schmid factors of the two component crystals, the plateau saturation stress of the bicrystal is in accord with that of copper single crystals oriented for single slip.

(2) The surface slip bands transferred through the GB on both surface I and surface II of the bicrystal, while secondary slip was not activated near the GB, indicating that the plastic strain near the GB was accommodated well in cyclic deformation. When the applied amplitude or cycle number was increased, a slight plastic strain incompatibility arose near the GB, but did not stimulate secondary slip.

(3) The ladder-like PSB structure can form in both grains during cyclic deformation, which is quite consistent with the CSS curve. On surface I, the ladder-like PSBs are continuous beside the GB, while the dislocation arrangements in those PSBs become irregular and discontinuous on surface II. Furthermore, a DAZ with a width of 5–10 μm was observed on the common primary slip plane on one side of the GB. In addition to the formation of the DAZ, there are three other kinds of interaction between dislocations, PSBs and the GB. Those observations indicate that the dislocations within the surface slip bands transferring through the GB are not perfectly continuous during cyclic deformation, even though the two grains have a common primary slip plane.

(4) The phenomenon of slip transfer through GBs is compared in fatigued crystals. It is suggested that both dislocations and PSBs cannot transfer through a random GB, irrespective of whether they are parallel, perpendicular or inclined to the stress axis. However, both PSBs and dislocations will pass through small-angle GBs perfectly. For the present bicrystal, the PSBs can only transfer partially through the GB, because the dislocations are not continuous across the GB. The piling up of dislocations at the GB should be attributed to the misorientation between the grains.

ACKNOWLEDGEMENTS

This work was financially supported by the National Natural Science Foundation of China under grant 59701006 and the Special Funds for the Major State Basic Research Projects G19990650. The authors are grateful for this support. In addition, the authors would like to express their appreciation to Professor C. Laird, Professor P. Lukas and Professor Z. R. Wang for their valuable comments and discussions.

REFERENCES

AHMED, J., WILKINSON, A. J., and ROBERTS, S. G., 1997, *Phil. Mag. Lett.,* **76**, 237.
BASINSKI, S. J., and BASINSKI, Z. S., 1989, *Acta metall.,* **37**, 3263; 1992, *Prog. Mater. Sci.,* **36**, 89.
CHENG, A. S., and LAIRD, C., 1981, *Mater. Sci. Engng,* **51**, 111.
ESSMANN, U., GÖSELE, U., and MUGHRABI, H., 1981, *Phil. Mag.* A, **44**, 405.
FINNEY, J. M., and LAIRD, C., 1975, *Phil. Mag.* A, **31**, 339.
GONG, B., WANG, Z. R., CHEN, D. L., and WANG, Z. G., 1997, *Scripta mater.,* **37**, 1605.
GOPALAN, P., and MARGOLIN, H., 1991, *Mater. Sci. Engng,* **A142**, 11.
HU, Y. M., WANG, Z. G., and LI, G. Y., 1996, *Mater. Sci. Engng,* **A208**, 260.
HU, Y. M., and WANG, Z. G., 1997a, *Acta mater.,* **45**, 2655; 1997b, *Scripta mater.,* **35**, 1019, 1997c, *Mater. Sci. Engng,* **A234–A236**, 98; 1998a, *J. Mater. Sci. Lett.,* **17**, 865; 1998b, *Int. J. Fatigue,* **20**, 463.
HUNSCHE, A., and NEUMANN, P., 1986, *Acta metall.,* **34**, 207.
JIA, W. P., LI, S. X., WANG, Z. G., LI, X. W., and LI, G. Y., 1999, *Acta mater.,* **47**, 2165.
LAIRD, C., 1996, *Physical Metallurgy,* Vol. III, fourth revised and enhanced edition, edited by R. W. Cahn and P. Haasen (Amsterdam: North-Holland).
LAIRD, C., CHARSLEY, P., and MUGHRABI, H., 1986, *Mater. Sci. Engng,* **81**, 433.
LEE, T. C., ROBERTSON, I. M., and BIRNBAUM, H. K., 1989, *Scripta metall.,* **23**, 779; 1990, *Phil. Mag.,* A, **62**, 131.
LI, X. W., HU, Y. M., and WANG, Z. G., 1998, *Mater. Sci. Engng,* **A248**, 299.
LIM, L. C., 1984, *Scripta metall.,* **18**, 1139.
LIM, L. C., and RAJ, R., 1985a, *Acta metall.,* **33**, 1577; 1985b, *ibid.,* **33**, 2205.
LUOH, T., and CHANG, C. P., 1996, *Acta mater.,* **44**, 2683.
MELISOVA, O., WEISS, B., and STICKLER, R., 1997, *Scripta mater.,* **36**, 1061.
MITCHELL, D. R. G., and DAY, R. A., 1998, *Scripta mater.,* **39**, 923.
MUGHRABI, H., 1978, *Mater. Sci. Engng,* **33**, 207.
PEDERSEN, O. B., RASMUSSEN, K. V., and WINTER, A. T., 1982, *Acta metall.,* **30**, 57.
PERALTA, P., and LAIRD, C., 1997, *Acta mater.,* **45**, 3029; 1998, *ibid,* **46**, 2001.
REPETTO, E. A., and ORTIZ, M., 1997, *Acta metall.,* **45**, 2577.
SCHWAB, A., BRETSCHNEIDER, J., BUQUE, C., BLOCHWITZ, C., and HOLSTE, C., 1996, *Phil. Mag. Lett.,* **74**, 449.
SCHWAB, A., MEIBNER, O., and HOLSTE, C., 1998, *Phil. Mag. Lett.,* **77**, 23.
SHEN, Z., WAGONER, R. H., and CLARK, W. A. T., 1986, *Scripta metall.,* **20**, 921.
SWEARENGEN, J. C., and TAGGART, R., 1971, *Acta metall.,* **19**, 543.
WALTERSDORF, J., and VEHOFF, H., 1989, *Scripta metall.,* **23**, 513.
WINTER, A. T., 1974, *Phil. Mag.* A, **30**, 719; 1978, *ibid.,* **37**, 457; 1981, *Acta metall.,* **29**, 735.
WINTER, A. T., PEDERSEN, O. B., and RASMUSSEN, K. V., 1981, *Acta metall.,* **29**, 735.
ZAUTER, R., PETRY, F., BAYERLEIN, M., SOMMER, C., CHRIST, H.-J., and MUGHRABI, H., 1992, *Phil. Mag.* A, **66**, 425.
ZHANG, Z. F., and WANG, Z. G., 1998a; *Phil. Mag. Lett.,* **78**, 105; 1998b, *Mater. Sci. Engng,* **A255**, 148; 1998c, *Acta mater.,* **46**, 5063; 1999, *Phil. Mag.* A, **79**, 741.
ZHANG, Z. F., WANG, Z. G., and HU, Y. M., 1999a, *Mater. Sci. Engng,* **A269**, 136; 1999b, *ibid.,* **A272**, 412.
ZHANG, Z. F., WANG, Z. G., and LI, S. X., 1998, *Fatigue Fracture Engng, Mater. Struct.,* **21**, 1307.